

# Supplementary Information

## Photoacoustic pigment relocation sensor

**Antonella Lauri<sup>1,2,4,‡</sup>, Dominik Soliman<sup>1,3,‡</sup>, Murad Omar<sup>1</sup>, Anja Stelzl<sup>1,2,4</sup>, Vasilis Ntziachristos<sup>1,3</sup> and Gil G. Westmeyer<sup>1,2,4\*</sup>**

<sup>1</sup>*Institute of Biological and Medical Imaging (IBMI), Helmholtz Zentrum München, Neuherberg, Germany*

<sup>2</sup>*Institute of Developmental Genetics (IDG), Helmholtz Zentrum München, Neuherberg, Germany*

<sup>3</sup>*Chair for Biological Imaging and* <sup>4</sup>*Department of Nuclear Medicine, Technical University of Munich (TUM), Munich, Germany*

<sup>‡</sup>*These authors contributed equally to this work*

\*Corresponding author: Gil G. Westmeyer

Email address: [gil.westmeyer@tum.de](mailto:gil.westmeyer@tum.de)

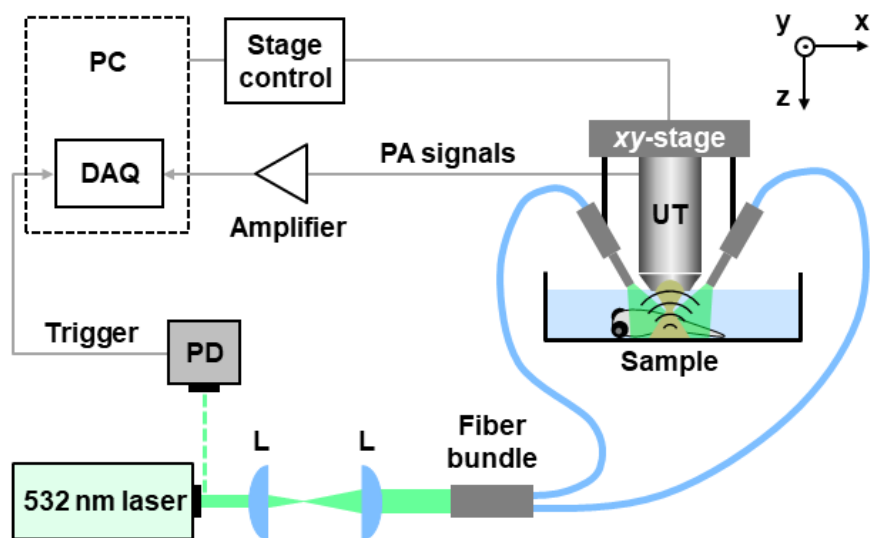


**Figure S1. Scheme of the RSOM system used in this study.** Abbreviations: DAQ, Data acquisition card; L, Lens; PA, Photoacoustic; PD, Photodiode; UT, Ultrasound transducer. Raster-scanning of the scanning head (ultrasound transducer and fiber bundle heads) was performed in the  $xy$ -plane while the sample remained stationary.

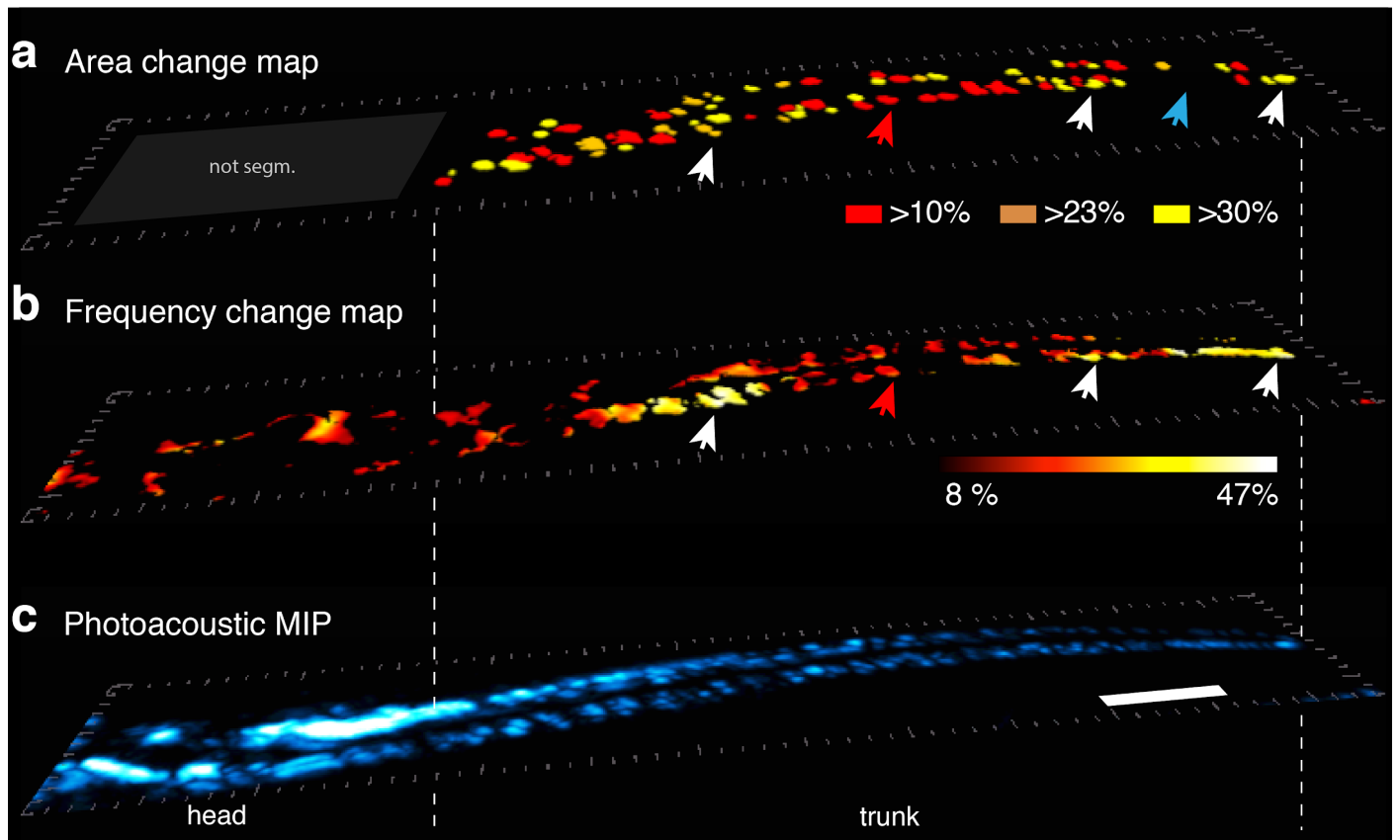


**Figure S2. Spatial mapping of photoacoustic frequency changes during background-adaptation-induced melanosome aggregation in a zebrafish larva *in vivo*.** (a) Melanophore clusters segmented from the MIP of the imaged zebrafish shown in panel c. The cell clusters are color-coded according to their reduction in area upon adaptation to a light background. The grey boxes indicate non-segmented regions ('not segm.'). Scale bar: 300  $\mu\text{m}$ . (b) Map of frequency shift magnitude in the same specimen after frequency analysis performed before and after adaptation to light background. White arrows indicate regions of strong frequency shifts and big area changes, the red arrow highlights an area exhibiting low frequency shifts. (c) Photoacoustic MIP of one of the dark-adapted zebrafish used here as anatomical reference. Segmentation was performed using the 'ROI Manager' plugin of Fiji. The single images were rotated in Imaris 7.7.

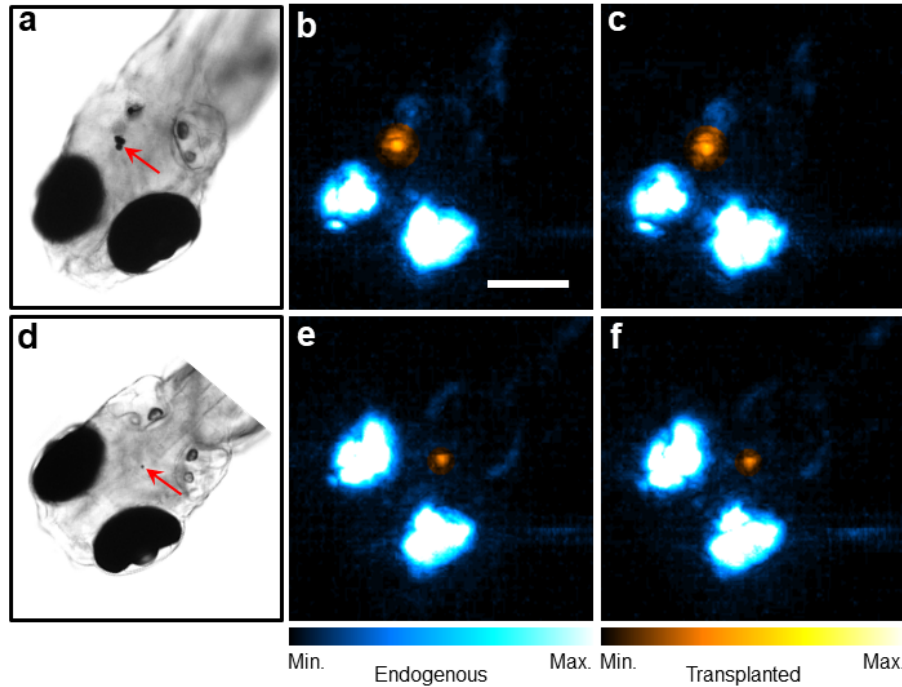


**Figure S3. Photoacoustic control measurements of a single transplanted *Xenopus* melanophore and a single transplanted microsphere in living zebrafish larvae.** (a-c) Transplanted *Xenopus* melanophore in a zebrafish (5-day-old rag2E450fs mutant) brain. **a**: Brightfield microscopy image of the transplanted melanophore inside the fish (red arrow). **(b,c)** Photoacoustic MIPs in top view of two consecutive measurements of the fish. **(d-f)** Transplanted 10  $\mu\text{m}$  black polystyrene microsphere (Polybead, Polysciences) in a zebrafish (rag2E450fs, 5-day-old) brain. **(d)** Brightfield microscopy image of the microsphere inside the fish (red arrow). **(e,f)** Photoacoustic MIPs (top view) of two consecutive measurements of the fish. Each pair of control measurements was performed with the same settings. Blue color map: native structures of the fish. Orange color map: circular region around the transplanted cell or microsphere. Scale bar: 400  $\mu\text{m}$ .

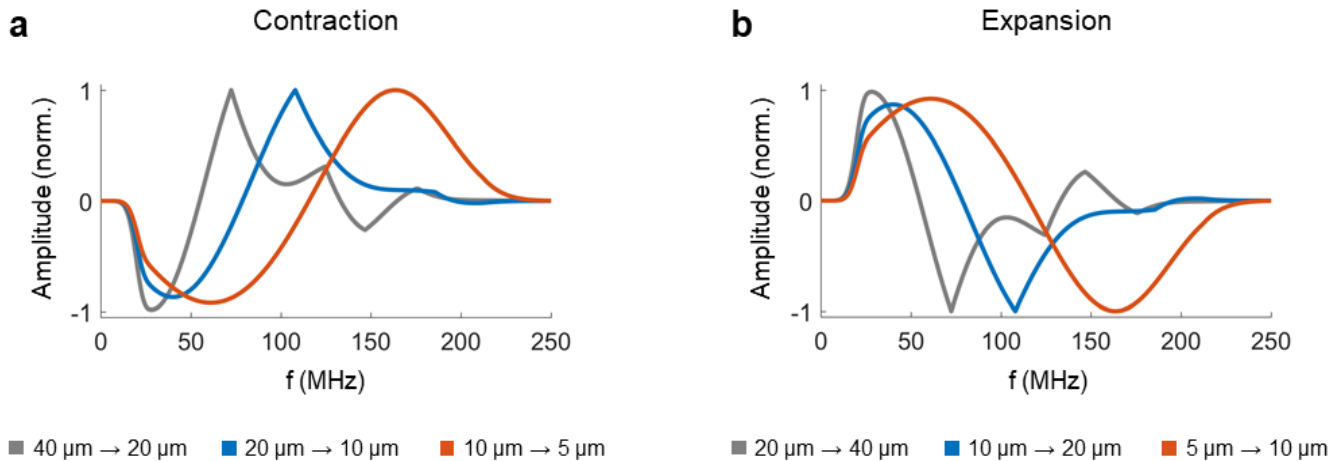


**Figure S4. Simulation of photoacoustic frequency difference spectra generated by spherical absorbers with changing size. (a)** Difference spectra (spectra of smaller spheres subtracted) for three different changes in size simulating contracting absorbers. **(b)** Difference spectra (spectra of larger spheres subtracted) for three different changes in size simulating expanding absorbers. Initial absorber diameters of 40, 20 and 10  $\mu\text{m}$  are illustrated in gray, blue and red colors, respectively.

## SUPPLEMENTARY MOVIES

**Movie S1:** 3D rotation of the reconstructed zebrafish shown in Figure 2a scanned with RSOM. Along the views perpendicular to the transducer axis, elongated structures such as the eyes can be observed. This anisotropic spatial resolution results from the limited angular acceptance of the transducer and the directivity of photoacoustic signals originating from elongated absorbers.

**Movie S2:** 3D rotation of the reconstructed zebrafish shown in Figure 4g scanned with MORSOM. Compared to RSOM reconstructions, MORSOM provides an isotropic spatial resolution in the plane perpendicular to the sample rotation axis.

## SUPPLEMENTARY METHODS

### Multi-orientation RSOM imaging

The multi-orientation RSOM (MORSOM) system employed the same laser as the RSOM modality. The imaging of the fish was performed after the melatonin stimulation experiment (see Figure 4g) and after final anesthesia. The specimen was mounted inside a column of agar with 4.5 mm diameter, which was immersed in a water tank. A syringe mounted to a rotational stage (RS-40, PI MICOS, Karlsruhe, Germany) held the agar column upside down. The rotation axis of the stage coincided with the axis of the agar column and rotated the sample by 360° in discrete steps. A spherically focused transducer (SONAXIS, Besancon, France; central frequency: ~50 MHz, bandwidth: ~10-100 MHz, focal distance: 3 mm, active element diameter: 3 mm) mounted in a horizontal orientation and facing the sample was raster-scanned in a plane parallel to the rotation axis. The sample was illuminated homogeneously from four directions by a fiber bundle (Ceram Optec GmbH). Each scan at a specific rotational position of the sample corresponded to an RSOM scan as described before was reconstructed individually and stored for further processing. After scanning the specimen at several angular positions within 360°, the different 3D reconstructions were combined yielding an isotropic spatial resolution of  $<20 \mu\text{m}$  in the plane perpendicular to the sample rotation axis (example shown in Supplementary Movie 2) and a spatial resolution along the rotation axis of  $\sim 44 \mu\text{m}$ . To facilitate the accurate combination of the different reconstructions, several  $10 \mu\text{m}$  black microspheres were embedded throughout the agar column holding the sample, serving as fiducial markers.

### Frequency analysis

For the frequency analysis of the photoacoustic data, the signals were bandpass filtered (a butterworth filter of order 2 with cutoff frequencies at 20 and 180 MHz was used) and the photoacoustic frequency spectra obtained by Fourier-transforming the time signals were summed up to form cumulative power spectra (CPS). For the *in vivo* experiments, the filtered photoacoustic signals used for the frequency analysis were selected according to their maximum amplitude in order to constrain the analysis to melanin related signals (signals originating from other sources or noise were assumed to yield lower amplitudes). Only photoacoustic signals with a maximum amplitude larger than 15% of the maximum amplitude value of the whole scan were selected. The resulting CPS, representing the summed-up thresholded frequency spectra of the whole scan, were smoothed using a moving average filter to remove fine fluctuations while keeping the global trend of the CPS. The individual CPS belonging to the control and stimulated scans of a certain experiment, respectively, were normalized to the areas under the curve. Finally, the difference spectra of two CPS (stimulated CPS minus control CPS) were calculated and normalized to the peak value of the respective control CPS.

The map of photoacoustic frequency shift magnitude shown in Supplementary Figure S2 was generated by processing the 3D reconstructions (as opposed to the raw time signals) of one of the specimens of the *in vivo* background adaptation experiment (see Figure 1). Due to the RSOM scanning geometry, the time axis of the photoacoustic signals corresponds to the depth dimension (z-axis) of the reconstruction. Therefore, by Fourier-transforming the z-signals of each xy-grid point of the 3D reconstruction, frequency spectra of each measurement position could be obtained. First, from the control measurement (dark-adapted state), melanin related signals were selected by discarding z-signals with a maximum amplitude value lower than 8% of the maximum amplitude value of the whole reconstruction, *i.e.*, setting them to zero in the frequency shift map. For each of the selected melanin-related z-signals corresponding to a certain measurement position in the xy-plane of the reconstruction, the frequency spectra of the z-signals of the surrounding neighborhood of 13

$\times 13$  signals were summed up to obtain local CPS. The CPS were assigned to the respective position at the center of the  $13 \times 13$  signals used for the calculation. The different local CPS were normalized to their peak amplitudes values instead of the areas under the curves for easier thresholding. For each local CPS of the dark-adapted fish reconstruction, a corresponding CPS was computed from the white-adapted fish reconstruction at the same  $xy$ -position and the respective difference spectra (white-adapted minus dark-adapted) were calculated. Further thresholding of the local difference spectra was performed in the frequency range of 70-200 MHz. If a difference spectrum had a negative minimum amplitude value or a maximum amplitude value lower than 8% of the respective control (dark-adapted) CPS peak, the corresponding pixel in the frequency shift map was set to zero. Otherwise, the pixel was assigned the peak amplitude value of the corresponding difference spectrum in the 70-200 MHz range. Finally, all pixels of the map were normalized to the maximum value of the whole frequency shift map.

### **Frequency shift simulations**

The optoacoustic signals used for the frequency shift simulation (Supplementary Figure S4) were generated with a MATLAB script assuming spherical fluid absorbers with different diameters. Acoustic attenuation in water, as well as the finite laser pulse duration, were incorporated in the simulation. The signals were further bandpass filtered as for the frequency analysis to model the transducer reception bandwidth. In order to produce difference spectra simulating shrinking or expanding absorbers, the frequency spectra of two signals corresponding to different absorber diameters were normalized to the areas under the curves and subtracted from each other. The resulting difference spectra for various initial diameters were normalized individually.